THE JOURNAL OF
PHYSICAL CHEMISTRY B
Article
pubs.acs.org/JPCB

Vibrational Properties of the Phosphate Group Investigated by Molecular Dynamics and Density Functional Theory

Valery Andrushchenko,* Ladislav Benda, Ondřej Páv, Martin Dračínský, and Petr Bouř*

Institute of Organic Chemistry and Biochemistry, Flemingovo náměstí 2, 16610, Prague, Czech Republic

Supporting Information

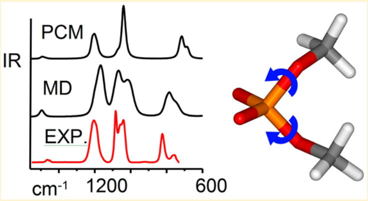

ABSTRACT: The phosphate group (PO_2^-) is an important building block occurring in many components of living matter including nucleic acids. It provides distinct features in vibrational spectra and is useful as a local probe of NA conformation and interactions with the environment. For this purpose, it is desirable to explore in detail various factors influencing spectral shapes of characteristic phosphate vibrations. In the present study, effects of the solvent and conformational averaging are analyzed for simple model molecules, dimethylphosphate, ethylmethylphosphate, and ethylmethylthiophosphate. Infrared absorption (IR) and Raman spectra were measured and calculated using a combination of molecular dynamics (MD) and density functional theory (DFT). To fully understand the link between the structure and the spectra, the solvent has to be explicitly included in the computational modeling. The results indicate that vibrational properties of the phosphate moiety are very sensitive to its conformation and interactions with the aqueous environment indeed. Polarizable continuum solvent models without explicit water molecules provided significantly worse agreement with the experiment. The combined MD/DFT approach captures well spectral characteristics for the model systems and constitutes the most reliable basis for exploration of phosphate vibrational properties in biomolecular structural studies.

■ INTRODUCTION

For a long time, vibrational spectroscopy has been revealing structural features of various biological components including nucleic acids (NA).[1−3] The information hidden in the shapes and positions of infrared absorption (IR), Raman scattering, vibrational circular dichroism (VCD),[4−6] or Raman optical activity (ROA)[7,8] bands can be deciphered by an empirical comparison of spectra of similar compounds. Later, computational chemistry including first-principles simulations provided more efficient and universal ways of spectra interpretation in terms of structural features. For example, simulations based on the simplified transition dipole coupling model (TDC)[9−11] and more elaborate density functional theory (DFT) approaches[12−15] made it possible to relate IR and VCD spectral shapes to standard DNA and RNA conformations.

In most studies, signal of nucleic acid bases has been analyzed only. This is understandable as these vibrations, predominantly the C═O and aromatic ring stretching modes, provide strong IR signal accessible with most spectrometers, and corresponding VCD spectral shapes faithfully reflect variations in the helical twist. However, the sugar−phosphate backbone gives specific spectral features as well. For the phosphate, many experiments indicate a tight connection between its vibrational spectra and NA conformations.[1,3,16] Being polar and positioned on the surface, the phosphate group also sensitively responds to NA interactions with the environment.[17,18] A principal objective of the present study thus includes estimation of the effect of PO_2^- hydration on spectral shapes, as the solvent−solute interaction may obscure the conformational information.

As the basic model, we adopt the dimethyl phosphate (DMP, $CH_3{-}O{-}PO_2^-{-}O{-}CH_3$) anion on which conformational and solvent factors affecting the spectroscopic response of the phosphate group can be studied in detail, both computationally and experimentally. Unlike for the nucleic acids and other larger molecules, DMP IR and Raman phosphate bands are not much overlapped with other vibrations. The molecular size allows for relatively accurate spectra simulations, based on a combination of molecular dynamics (MD) and quantum mechanics (QM).

In the past, vibrational properties of the phosphate group were addressed using DFT computations in vacuum[19] or exploring a dielectric model of the aqueous environment.[20] However, many studies indicate that the simplified solvent models do not fully account for strong polar interactions,[21,22] such as those occurring between the phosphate solute and water.[23] The necessity to properly involve the dynamics and solvent in the simulations was observed for NA properties as well.[14,15,24−26] Although reasonably accurate for the nitrogen base region, the dielectric solvent approach was found to be inadequate for the phosphate group.[14] In addition, a static involvement of several "explicit" solvent molecules in the spectral simulations may not be sufficient. As shown below, averaging of a reasonable number of MD clusters with different water positions is necessary for a reliable description of observable spectral features.

Received: May 29, 2015
Revised: July 18, 2015
Published: July 20, 2015

ACS Publications

DOI: 10.1021/acs.jpcb.5b05124
J. Phys. Chem. B 2015, 119, 10682−10692

The second small molecule studied here is ethyl methyl phosphate (EMP). In fact, it provides very similar spectra as DMP, confirming the locality of the strongest phosphate vibrations. EMP is also interesting from the computational point of view, as the additional degree of conformational freedom (ethyl group rotation) might have an impact on cluster averaging, and the methyl/ethyl substitution in a primitive way mimics the incorporation of the phosphate group into a longer sugar−phosphate NA chain.

The third ethyl methyl thiophosphate (EMSP) model does not contain the PO_2^- group at all; however it is valuable for validation of the robustness of the methodology on a chemically similar moiety. In addition, the thio-analogues of the phosphate exhibited an interesting potential for the pharmaceutical industry.[27] Phosphate group derivatives play also a significant role in the regulation of gene expression; modified oligonucleotides proved to be powerful tools in treatment of various diseases. As of the year 2014, for example, two antisense oligonucleotides Fomivirsen (marketed as Vitravene) and Mipomersen (marketed as Kynamro) were approved by the U.S. FDA for the treatment of cytomegalovirus-induced retinitis and familial hypercholesterolemia.[27,28] Both these oligonucleotides are based on the nucleoside thiophosphate.

During the simulations, we use the polarizable continuum methodology[29] as well as averaging of many solvent solute clusters. The latter approach combining quantum and classical mechanics established as a standard and highly flexible way of simulating spectral properties of hydrated molecules.[30,31] Because of limited computational sources (for ab initio MD) and precision of classical MD force field we did not generate the spectra directly from MD trajectories by Fourier transform.[32,33] However, this approach is mentioned as it previously provided equally faithful description of strongly hydrated molecules in water solutions, including those with the phosphate moiety.[34,35]

■ METHODS

Experimental Section. EMP and EMSP were synthesized from DMP and ethyl dichlorothiophosphate, respectively. Details of the synthesis can be found in Supporting Information. DMP, NaCl, NaOH, and D_2O (99% purity, ACS grade) were purchased from Sigma-Aldrich. The studied molecules and definition of the torsion angles based on standard notation used for NA are plotted in Figure 1.

All samples were dissolved at 0.135 M concentration in Milli-Q water or in D_2O. H_2O solutions were used to acquire spectra above 1000 cm^{-1}, whereas D_2O was used below 1000 cm^{-1} because of the strong absorption of H_2O in this region. IR spectra of DMP were measured with an Equinox 55 FTIR spectrometer (Bruker Optics, Inc.). IR spectra of EMP and EMSP were acquired with a Nicolet 6700 spectrophotometer (Thermo Fisher Scientific Inc.). For each compound, 256 scans were collected at 4 cm^{-1} resolution at room temperature, using BaF_2 cell with optical path length of 37 μm.

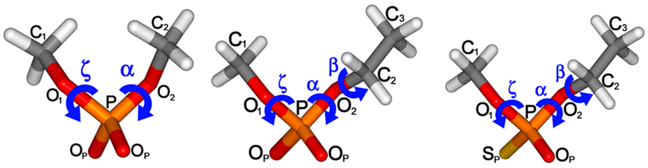

Figure 1. Three model compounds, DMP (left), EMP (center), and EMSP (right), and definition of characteristic torsion angles $\zeta = \angle(C_1{-}O_1{-}P{-}O_2)$, $\alpha = \angle(C_2{-}O_2{-}P{-}O_1)$, and $\beta = \angle(C_3{-}C_2{-}O_2{-}P)$.

Raman spectra were measured with a ChiralRAMAN-2X spectrometer (BioTools Inc.) equipped with an Opus diode-pumped solid-state laser operating at 532 nm. The laser output power was set to 700 mW (about 350 mW at the sample). Sample solutions were contained in fused silica cell (3 mm × 3 mm, containing 80 μL of solution) and the spectra were accumulated for 20 min.

Molecular Dynamics Simulations. MD input geometries were prepared using the *tleap* module of Amber program;[36] atomic partial charges in DMP, EMP and EMSP were obtained from the R.E.D. server.[37−39] Studied molecules were placed in rectangular boxes filled with water (674 water molecules for DMP, 733 for EMP, and 778 for EMSP). Total charge of each system was −1. For comparison, a neutral DMP box with one Na^+ ion and 714 water molecules was prepared as well, using an analogous procedure. All MD simulations used the periodic boundary conditions.

Equilibration, production MD simulations, and trajectory analyses were performed with the *sander* and *ptraj* modules of Amber 10.[40] The PARM99/PARMBSC0 (referred to as Amber99)[41] and general Amber force field (GAFF) were used for DMP; EMP and EMSP simulations were performed with GAFF only. The TIP3P force field[42] was used for water. After a sequence of restrained minimizations and heating, 100 ps equilibration dynamics was performed at 300 K without any restraints. The box sizes after the equilibration of the *NPT* ensembles were 26.4 × 28.7 × 27.0, 29.8 × 28.1 × 26.8, and 30.7 × 28.3 × 27.5 $Å^3$ for DMP, EMP, and EMSP simulations, respectively. Langevin thermostat with the collision frequency of 1 ps^{-1}, the SHAKE algorithm with a tolerance of 10^{-5} Å, 2 fs integration time step, Lennard-Jones interactions with a cutoff at 10 Å, and the particle mesh Ewald method (PME) were used.

A production MD was run for 50 ns at 300 K. To separate the effects of water dynamics and conformation on the spectra, shorter 1 ns MD simulations were performed for the same system and conditions but with DMP torsion angles ζ/α fixed to the major conformer values, that is, 60°/60° (gg), 60°/180° (gt), and 80°/280° (gg^-) for Amber99 and 80°/80° (gg), 80°/180° (gt), and 80°/240° (gg^-) for GAFF, applying a penalty harmonic potential with a force constant of 10 kcal mol^{-1} $Å^{-2}$. The abbreviations gg, gt, and gg^- stand for gauche−gauche, gauche−trans, and gauche−gauche$^-$.

Free energy (ΔG) dependence on the torsion angles was obtained as a potential of mean force using the weighted histogram analysis method (WHAM);[43] both ζ and α were incremented by 20° and at each point a harmonic force constant of 15 kcal $mol^{-1}rad^2$ was applied, providing an overlap of the sampled conformations by ca. 70%. At each point a production run was performed for 100 ps, the pressure relaxation time was set to 5 ps, and the integration time step to 1 fs. Other parameters were the same as for the unrestrained MD. For EMP and EMSP, the torsion angle β was left to evolve freely.

Ab Initio Molecular Dynamics. Born−Oppenheimer molecular dynamics (BOMD) of DMP and EMSP was performed with the CPMD program.[44] The DMP or EMSP molecule with a charge of −1 was placed in a cubic box 10.1 and 10.2 Å wide, respectively, and 27 water molecules were

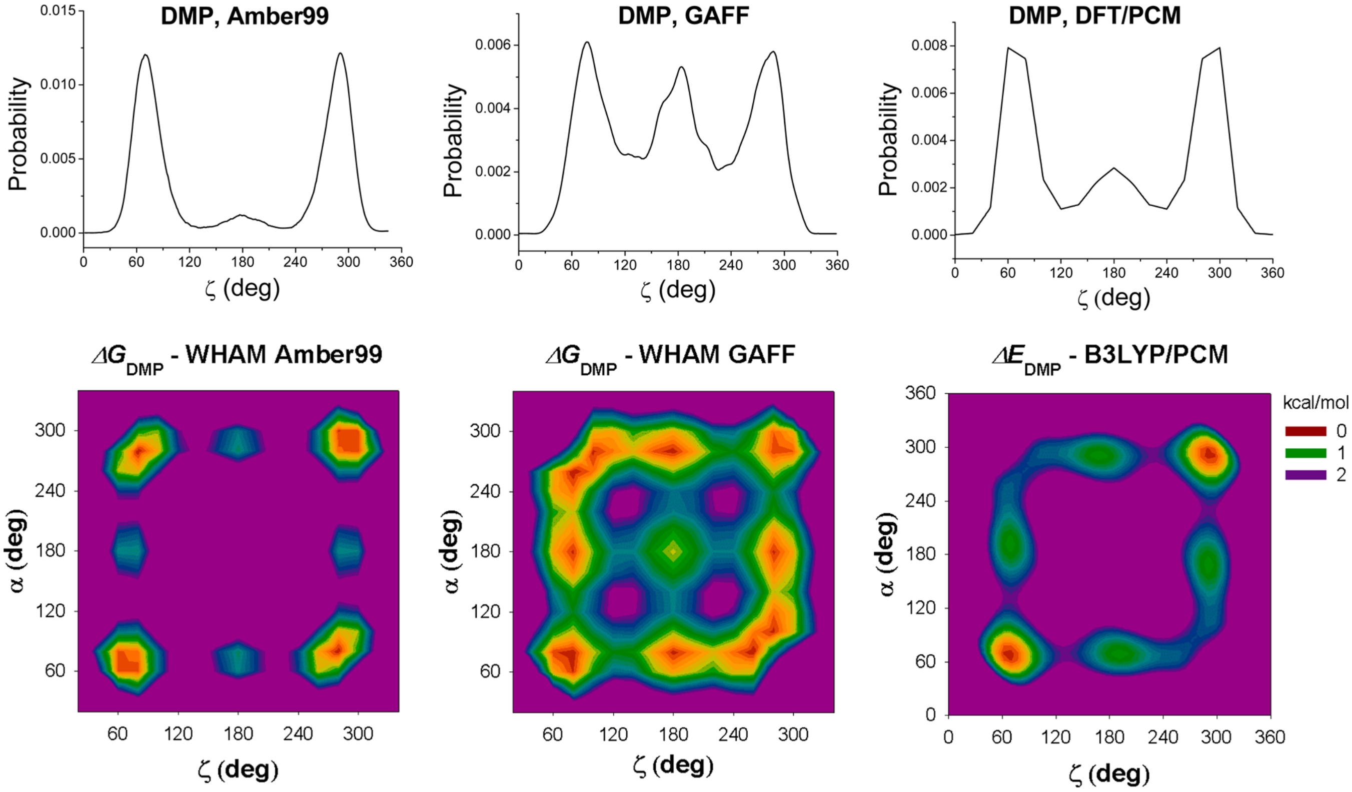

Figure 2. Two-dimensional potential energy surfaces of DMP as obtained by the Amber99, GAFF, and B3LYP/6-311++G**/PCM computations. Integrated one-dimensional distributions dependent on the ζ angle are plotted at the top.

added. The BLYP[45] functional was used and the plane wave basis set was cut off at 340 eV. The simulations ran for 150 and 100 ps for DMP and EMSP, respectively. The simulation times were too short to provide balanced conformer distributions; however, the BOMD allowed us to estimate radial distribution function of the solvent in the vicinity of the solute and compare it to the classical MD result.

DFT Simulations with Implicit Solvent. A systematic conformer search was performed for the DMP, EMP, and EMSP molecules, and the geometries of local minima on the potential energy surface (PES) were optimized with several methods, using the Gaussian 09[46] and TurboMole 6.3.1[47] programs. For DMP, PES was also explored by varying the torsion angles ζ and α in 20° steps and optimizing the rest of coordinates at each point. The B3LYP[48] functional and 6-311++G** basis set were used as a default. The solvent was included via polarized continuum model (PCM), conductor-like solvent model (COSMO, including its Gaussian implementation "CPCM")[49−51] and COSMO-RS method[52] with σ-potential of water at 298.1 K. van der Waals interactions were included via the Grimme's D3 correction[53] with Becke-Johnson's (BJ) damping[54] (D3BJ). Vibrational frequencies and IR and Raman spectra were calculated at the same level as optimized geometries. Gibbs free energies were obtained within the standard ideal-gas rigid-rotator harmonic oscillator model.[55] The DFT/CPCM conformer spectra were averaged using the MD energies, better describing the strong solvent−solute interactions than the CPCM model. However, control computations indicated that resultant spectra shapes were fairly independent of the weighting scheme. No scaling of DFT frequencies was done, as it may obscure the solvent effect, and even multifactor scaling schemes usually bring about a uniform shift of calculated frequencies only.[56] Excitation wavelength of 532 nm was used for response calculations of the Raman spectra.

Generating Spectra with MD Clusters. For each system, 300 snapshots evenly separated along a 50 ns MD trajectory were selected for the averaging. Test computations (Figure S1) indicated that this number of snapshots provides sufficiently accurate spectra. Only solvent molecules H-bonded to the solute (typically 7−8 waters, example geometries are plotted in Figure S2) were kept in the snapshots for DFT calculations. As computations of vibrational spectra on raw MD clusters are meaningless,[57−59] the snapshots were partially optimized in vibrational normal mode coordinates[60] using the QGRAD program.[60] Low-frequency (<300 cm^{-1}) normal modes were frozen, which resulted to a minor perturbation of the MD geometry only. Then the spectra were calculated for all snapshots by Gaussian 09 and final shapes obtained as a plain average of all MD snapshots. The B3LYP/6-31++G**/CPCM method was used as it provided reliable vibrational spectra of similar systems previously.[15] For simulation of spectral curves Lorentzian profiles were used with the full width at half-maximum of 10 cm^{-1}.

■ RESULTS AND DISCUSSION

Conformer Energies and Potential Energy Surfaces. The molecules exhibit a relatively limited number of conformers; their geometry and relative energies are summarized in Table S1. Vacuum and dielectric solvent results are consistent with previous studies.[19,20] For example, vacuum B3LYP/6-31G* computation predicted[19] equilibrium value α = 70° for the gg conformer; our computation (B3LYP/6-31++G**) predicts 74°, which changes to 68−65° in the solvent,

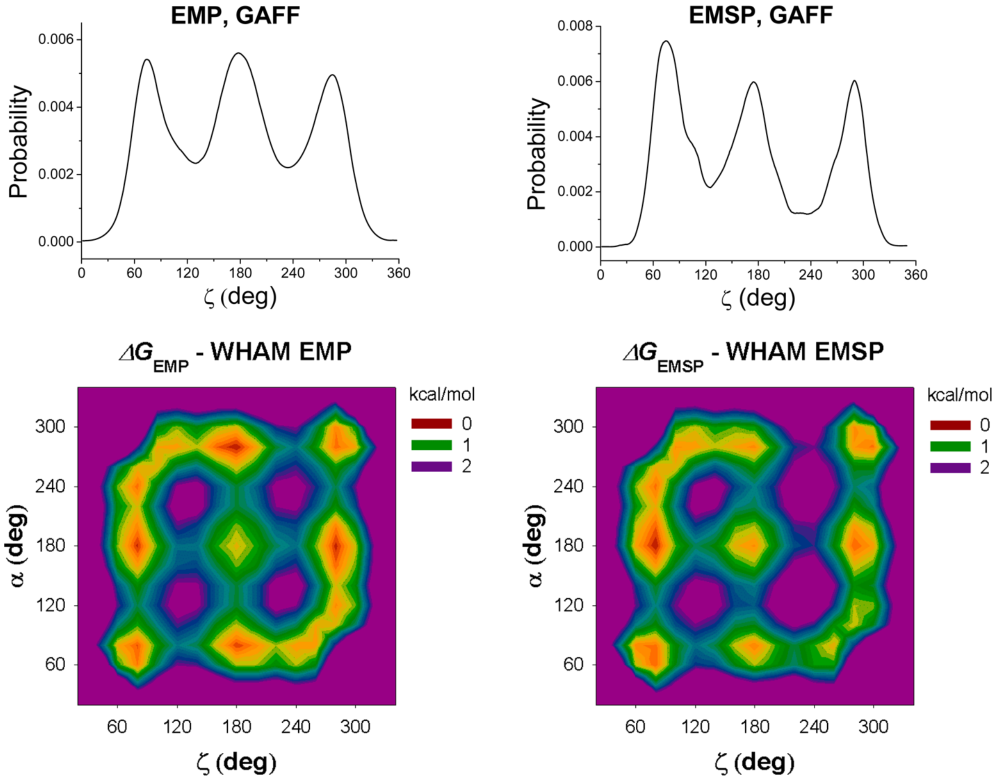

Figure 3. Mean-force Amber99 potential of EMP (left) and EMSP (right) with integrated ζ−probabilities plotted above.

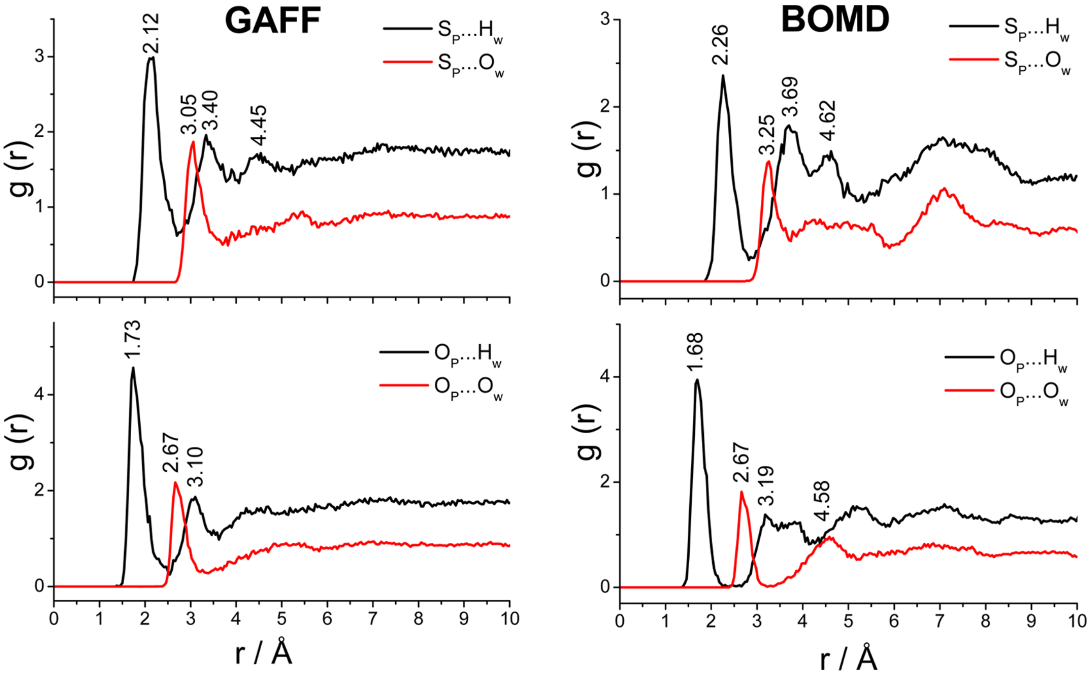

Figure 4. EMSP radial distribution functions of water oxygen (O_W) and hydrogen (H_W) as obtained with the classical (GAFF) and ab initio (BOMD) dynamics.

according to the dielectric model adopted. For DMP, the dispersion correction does not change the conformer ordering.

The MD simulations provide more variable results and indicate that the geometry is more flexible than obtained by the static DFT models. The dependence of the free (obtained for Amber99 and GAFF force fields) and electronic (B3LYP/6-311++G**/PCM) energy on the ζ and α angles for the entire DMP PES is plotted in Figure 2 with separate histograms for the ζ angle. All methods predict a local minimum around 60°/60° (gg conformer of C_2 symmetry), energy of which is the same as for the 300°/300° (g^-g^-) conformer. The Amber99 force field provides another minimum at 80°/280° (= 280°/80°) (gg^- = g^-g) of C_s symmetry and a very weakly populated "C_1" minimum at 60°/180° (= 180°/60°) (gt = tg). The GAFF

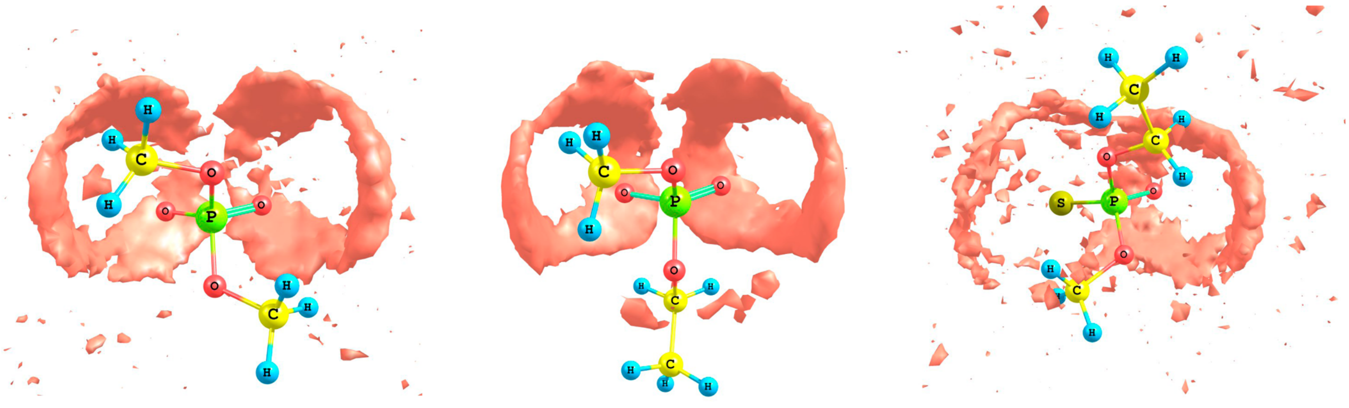

Figure 5. Structure of the first hydration shell (water isodensity) around DMP (left), EMP (middle), and EMSP (right) molecules, GAFF calculation.

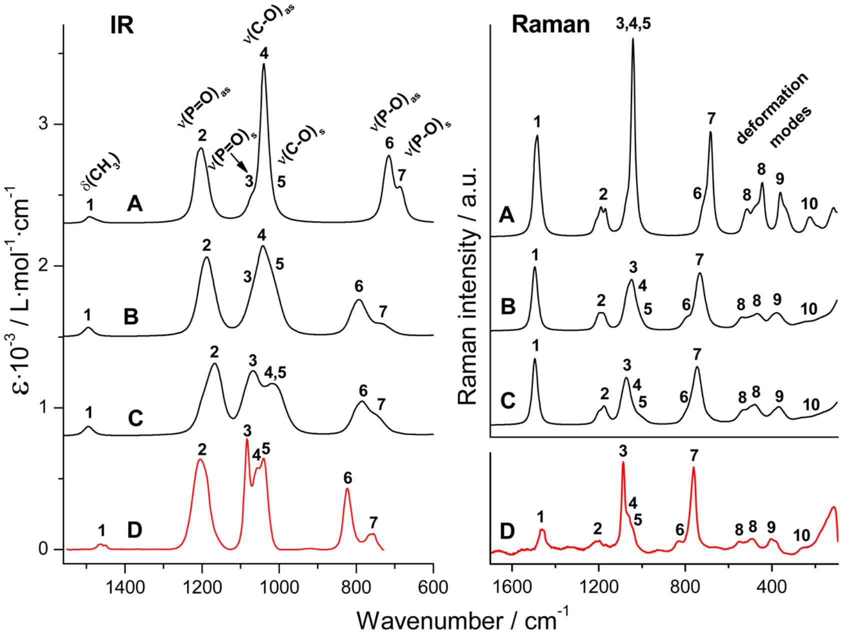

Figure 6. IR (left) and Raman (right) spectra of DMP. (A) DFT/CPCM spectra of 324 conformers Boltzmann-averaged according to the GAFF population probabilities; (B) MD/DFT cluster averages from 300 Amber99 MD snapshots; (C) MD/DFT cluster averages from 300 GAFF MD snapshots; (D) experiment. Experimental IR spectrum below 1000 cm^{-1} was measured in D_2O, which is more transparent in that spectral region than H_2O. The band assignment is summarized in Table 1.

force field provides a more even conformer distribution than Amber99 with lower energy barriers between them. The "gg-" conformer provides two minima with GAFF at 80°/255° and 90°/285° (plus the symmetric counterparts), and a fully extended form appears at 180°/180° (tt, of C_{2v} symmetry).

Note that the gg and tg conformers correspond to phosphate geometries in B_I and B_{II} conformations of DNA, respectively; the gg- conformation does not occur in canonical B-DNA.[61−63] This may explain the differences between the Amber99 and GAFF results. Only the Amber99 force field was parametrized to stabilize canonical *B*-DNA, whereas GAFF was designed for general purposes and in our case allows for higher flexibility of DMP. Therefore, it might provide more realistic results for the systems studied here, as observed below indeed.

In comparison with MD, the DFT computation provides the most rigid geometry with domination of the gg conformer. MD simulations with the Na^+ counterion provided very similar results and are not shown. This is consistent with the minor effect of sodium ions at low concentrations on DMP energetics and vibrational spectra, as was reported also by other authors.[19,64]

The EMP provides virtually the same ζ/α energy landscape as DMP (left-hand side of Figure 3, only the GAFF result is shown), with similar conformer ordering (E(gg) < E(gt) < E(gg-)) provided by DFT/CPCM calculations (Table S1). The EMSP potential energy surface (Figure 3, right-hand side, and Table S1) is not symmetric; the ggt minimum is significantly more populated than the g-g-t one, and the extended ttt conformer is more populated than the corresponding tt DMP form. The β-torsion angle exhibits a simple narrow distribution (not shown) centered around 180°, which is in agreement with its value in the DNA backbone.[63] Interestingly, the conformer ordering for EMSP is different compared to DMP and EMP. The most stable conformer in EMSP is gtt (Table S1), which was also indicated by previous computational and experimental studies.[20,65] Energy differences between EMSP conformers are relatively low, mostly within 1 kcal/mol. The extended ttt conformer appears to be as stable as the gg-t.

Table 1. Experimental and Computed Frequencies of Selected DMP, EMP, and EMSP vibrational bands[a]

	IR		Raman		
peak	$\nu_{\mathrm{Exp.}}$	$\nu_{\mathrm{Calc.}}$	$\nu_{\mathrm{Exp.}}$	$\nu_{\mathrm{Calc.}}$	assignment
DMP (Figure 6)					
1	1464	1495	1465	1494	$\delta(CH_3)$
2	1205	1167	1205	1175, 1202_{sh}	$\nu(P{=}O)_{as}$
3	1083	1068	1087	1072	$\nu(P{=}O)_{s}$
4	1056		1060_{sh}	1064_{sh}	$\nu(C{-}O)_{as}$
5	1041	1019	1038_{sh}	1015_{sh}	$\nu(C{-}O)_{s}$
6	824	785	829	803_{sh}	$\nu(P{-}O)_{as}$
7	760	746_{sh}	762	745	$\nu(P{-}O)_{s}$
8–9			551, 493, 405, 383, 248	531, 479, 391, 370, 265 (respectively)	deformation modes
EMP (Figure 7)					
1	1449	1493	1458	1491	$\delta(C_1H_3)$
1′	1395	1432	1399, 1294	1435, 1319	$\delta(C_2H_2{-}C_3H_3)$
2	1202	1171	1198	1176	$\nu(P{=}O)_{as}$
3	1081	1075_{sh}			$\nu(P{=}O)_{\mathrm{s}} + \nu(C{-}O)_{s}$
3	1058	1055	1086	1078	$\nu(P{=}O)_{\mathrm{s}} + \nu(C_1{-}O_1)$
4	1040	1031_{sh}	1043_{sh}	1046_{sh}	$\nu(P{=}O)_{\mathrm{s}} + \nu(C{-}O)_{as}$
5	953	941	952	956	$\nu(C_2{-}O_2)$
6	818	796	817	800_{sh}	$\nu(P{-}O)_{as}$
7	753	750_{sh}	759	757	$\nu(P{-}O)_{s}$
8–9			551,530, 492, 396, 351	546, 509, 475, 389, 342	deformation modes
EMSP (Figure 8)					
1	1447	1492	1458	1490	$\delta(C_1H_3)$
1′	1392	1427	1398, 1290	1432, 1314	$\delta(C_2H_2{-}C_3H_3)$
2	1132	1114	1134, 1104	1170, 1117	$\nu(P{=}O)$
3	1024	1029	1046	1029	$\nu(C_1{-}O_1) + \nu(C_2{-}O_2)$
4	947	940	948	940	$\nu(P{-}O_2)$
5	774	778	782	783	$\nu(P{-}O_1)$
6			647, 616	631	$\nu(P{=}S)$
7–8			445, 326	443, 337	deformation modes

[a] Frequencies are given in cm^{-1}, computed values are from the GAFF/DFT cluster average spectrum, *as* and *s* denote locally asymmetric and symmetric vibrations, *sh* is a shoulder, experiment relates to H_2O solutions

Hydration and Solvent Radial Distribution Function. The negatively charged phosphate moiety interacts strongly with the aqueous environment. We were in particular interested in how well a classical nonpolarized MD force field describes the hydration in comparison with the ab initio dynamics, that is, whether it provides a realistic water distribution around the solute. As shown previously, correct water distribution and its dynamics are among the most crucial points in correct modeling of vibrational spectra.[14,15,25] The radial distribution functions obtained with the GAFF force field and BOMD are compared for EMSP in Figure 4. Apparently, very similar hydration patterns within the first hydration shell are obtained by the two approaches. The BOMD simulation predicts the S···H bond to be ~2.26 Å by 0.14 Å longer than GAFF; on the contrary, the BOMD O···H bond length (1.68 Å) is by 0.05 Å shorter than GAFF. However, because the MD bond lengths and angles need to be optimized at QM level for computation of the vibrational spectra, the small differences do not affect the modeling. In another representation, the structure of the first hydration shell for DMP, EMP, and EMSP molecules is shown as the isodensity plots in Figure 5. As expected, DMP and EMP provide a very similar pattern (Figure S3). In EMSP, the S···H_2O hydrogen bonds are weaker (~0.5 Å longer than O···H_2O ones), and the first hydration shell around the sulfur atom is less compact.

Vibrational Spectra of DMP. Experimental and computed IR and Raman spectra of DMP are shown in Figure 6, and peak positions and assignments of the most intense bands are summarized in Table 1. The experimental IR spectrum is dominated by the asymmetric (out-of-phase) and symmetric (in-phase) P═O stretching vibrations at 1205 and 1083 cm^{-1}, respectively, marked as bands 2 and 3 in Figure 6. The asymmetric and symmetric stretching C–O bands 4 and 5 appear close to the symmetric ν(P═O) band, while ν(P–O) asymmetric and symmetric modes 6 and 7 around 800 cm^{-1} are separated from the others. A visualization of the normal mode displacement confirmed that the asymmetric P═O stretching is rather uncoupled to other molecular coordinates, whereas symmetric P═O, P–O, and C–O stretches mix. A weak CH_3 group deformation band 1 appears at 1464 cm^{-1}. Relative Raman intensities differ from IR; asymmetric ν(P═O) and ν(C–O) bands are weaker while the symmetric ν(P–O) band and symmetric CH_3 deformation mode is stronger than in IR.

All computational methods (traces B–C in Figure 6) reasonably well reproduce the main experimental features in IR and Raman spectra, that is, the dominant symmetric and asymmetric P═O stretching regions, separated from the C–H bending and P–O stretching vibrations. However, significant frequency and band shapes inconsistencies appear according to the simulation method used. The fine splitting of bands 3–5 is reproduced by GAFF cluster averaging (trace C) only. IR C–O stretching bands 4 and 5 are separated from the phosphate symmetric P═O stretching 3, while they appear as a shoulder in the Raman spectrum only, which is reproduced by the GAFF simulation as well. The simulation based on the Amber99 force field (trace B) provides some of these features, although not so well as GAFF. The success of GAFF suggests again that this force field is better suitable for description of DMP dynamics than Amber99.

These results are consistent with previous modeling of DNA IR spectra, where an explicit hydration significantly improved the symmetric P═O and C–O stretching pattern (1000–1100 cm^{-1}) if compared with a vacuum simulation.[12,24] For DNA quadruplexes[15] or deoxyguanosine monophosphates,[25] a polarizable solvent model also led to a larger error in calculated frequencies (~30–40 cm^{-1} if compared to the experiment) than the MD cluster methodology used in the present study (~15 cm^{-1}). The phosphate vibrations behave similarly in RNA[13] and DNA and are easily identifiable in both molecules. The asymmetric P═O stretching band is relatively isolated and less coupled with other modes. Its position is sensitive to conformation, and it is thus used as a marker. The symmetric P═O stretching signal is less sensitive to conformational changes and more coupled. Because of the coupling, its band shape is different in DNA, RNA, or single-/double-/triple-/quadruple-stranded structures.[13,15]

The plain DFT-based simulation with the continuum solvent model only (trace A) gives the worst agreement. The inclusion of the solvent molecules and averaging of solvent configurations

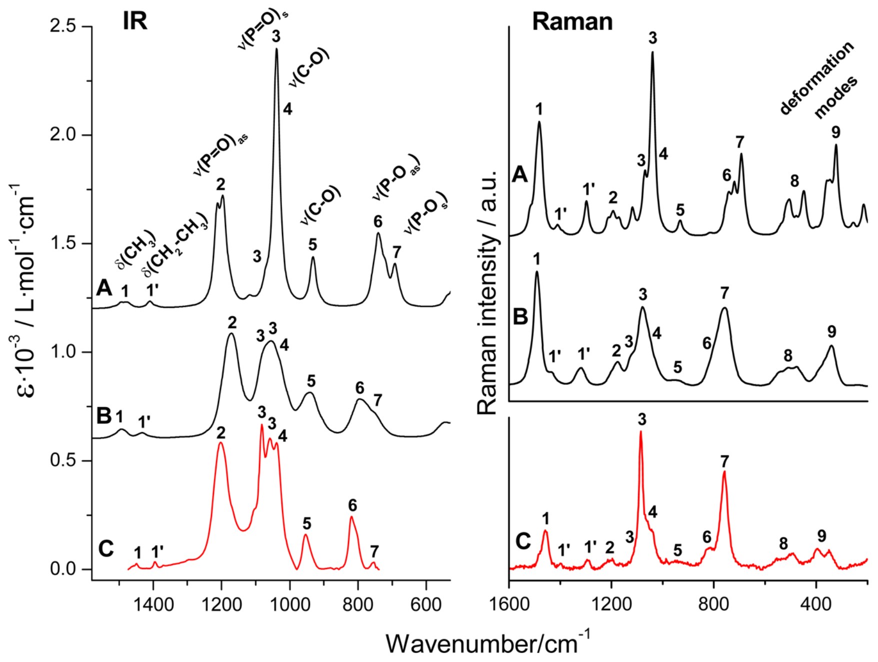

Figure 7. Experimental and simulated IR and Raman spectra of EMP. (A) DFT/CPCM spectra of 27 conformers Boltzmann-averaged according to the GAFF population probabilities; (B) MD/DFT cluster averages from 300 GAFF MD snapshots; (C) experiment. Experimental IR spectrum below 1000 cm^{-1} was measured in D_2O. Assignment of the labeled bands is summarized in Table 1.

is thus mandatory for a faithful reproduction of the experiment. In the DFT/CPCM approach, all asymmetric modes (2, 4, and 6) provide too strong IR and too weak Raman bands, while the symmetric modes (1, 3, 5, and 7) exhibit too weak IR and too strong Raman bands (spectra A in Figure 6). It is interesting that the P−O (single-bond, bands 6 and 7) stretching frequencies are computed with a large error (∼50 cm^{-1}) with this method, larger than for the more "polar" P═O stretching modes. For the principal PO_2^- vibrations, the Raman spectra appear to be less sensitive to the computational approach, conformational and environmental modeling than IR. This, however, should not be generalized; indeed, the lower-wavenumber deformation modes (8−10) exhibit slightly larger variations.

To understand the origin of the band broadening and to separate the conformational and environmental effects, we performed a set of restrained MD simulations with DMP geometry fixed in major conformations, averaging water positions only. The individual conformer spectra showed subtle variation, while their averaging (red traces in Figure S4) provided similar results for Amber99 and GAFF in this case. On the other hand, spectra of individual snapshots in Figure S5 exhibit much larger variations and demonstrate that water configuration has a significant effect on the spectral shapes.

Note that the bandwidth in the DFT/CPCM computations (e.g., traces A in Figure 6) is an arbitrary number; in the cluster-based simulations it is somewhat smoothed by the convolution with the Lorentzian bands, too, but the main broadening comes from the solvent−solute interactions and geometry dispersion (cf. Figures S4 and S5). For modes 3−7, the MD averaging predicts broader bandwidths than observed experimentally, indicating that both the Amber99 and GAFF force fields provide potentials that are too "shallow".

Because the IR intensity of $\nu(P{=}O)_s$ (3) and $\nu(C{-}O)$ (4 and 5) bands in individual conformers differ, the IR spectrum provides information about the conformer ratios. The gg conformer is connected with higher intensity of bands 4 and 5, while gt and especially gg$^-$ conformers are connected with increased intensity of band 3 (Figure S4). The shape of the experimental IR spectrum where band 3 is more intense than 4/5 (Figure 6) implies that gt and gg$^-$ DMP conformers outnumber gg. These marker bands thus appear generally useful for phosphate studies. For example, in our earlier IR study of deoxyguanosine monophosphate (dGMP),[25] the bands 4/5 were more intense than 3 (see Figure 7 in ref 25), which suggests a larger contribution of the gg conformer.

Also the $\nu(P{=}O)_{as}$ IR band 2 is sensitive to the DMP geometry. Position of this band in gg and gt (Figure S4) differs by about 19 cm^{-1} (GAFF). The $\nu(P{=}O)_{as}$ band is frequently used as a sensitive indicator of transitions between B, A, and Z DNA forms.[66] In particular, the B−Z transition is accompanied by a large 10 cm^{-1} shift of this band.[1,16,67−69] Unlike the right-handed B-DNA, which adopts the g$^-$g$^-$ backbone conformation (equivalent to gg in DMP), the left-handed Z-form has alternating gg/g$^-$t values of ζ- and α-torsion angles.[20,62,70] Thus, compared to B-DNA the $\nu(P{=}O)_{as}$ band in Z-DNA should be shifted to lower wavenumbers by about half the difference between its position for gg and gt conformers. The predicted GAFF value of 9.5 cm^{-1} is in excellent agreement with the experimentally observed shift.

In another control computation, we completely removed the hydration shell for major DMP conformers (Figure S6). The overall DFT/CPCM spectral band shapes are not as realistic as with the explicit water molecules, but the main trends in conformational variations of the spectra are conserved. Although the intensity of the $\nu(P{=}O)_s$ IR band 3 is very low for the gg conformer, it increases for gt and gg$^-$. The shift of the $\nu(P{=}O)_{as}$ IR band 2 between gg and gt conformers is also modeled correctly, although slightly underestimated. Thus, the spectral changes are intrinsically dependent on the DMP conformation and only enhanced by the presence of the solvent.

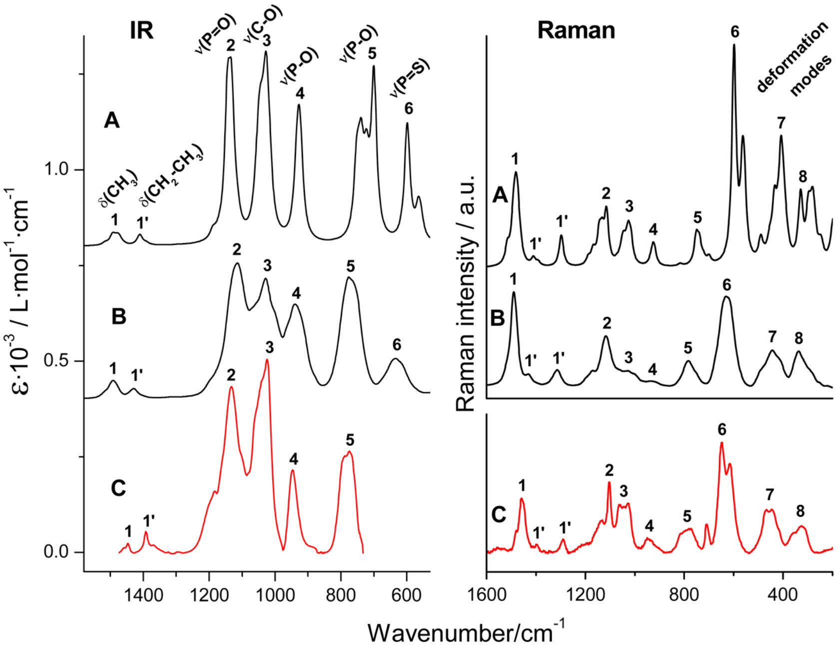

Figure 8. Experimental and simulated IR and Raman spectra of EMSP. (A) DFT/CPCM spectra of 27 conformers Boltzmann-averaged according to the GAFF population probabilities; (B) MD/DFT cluster averages from 300 GAFF MD snapshots; (C) experiment. Experimental IR spectrum below 1000 cm^{-1} was measured in D_2O.

A typical accuracy of the computed harmonic vibrational frequencies if compared to experiment (Table 1) is 3−35 cm^{-1}, which may be caused by a limited accuracy of the B3LYP functional,[71] neglect of the anharmonic potential contributions[72,73] and approximations adopted in the treatment of the solvation. This error is rather minor and it does not prevent us to assign and understand most of the phosphate vibrations. It is interesting that the negative charge and the overall polarity of the PO_2 do not have an extreme effect on vibrational properties. For example, inclusion of the solvent in the computations changes the P═O vibrational frequencies by 20−40 cm^{-1} if compared to vacuum,[19] which is less than for the similarly polar but neutral C═O groups where solvation-induced shifts up to ∼65 cm^{-1} were predicted.[74]

Vibrational Spectra of EMP and EMSP. For EMP, the calculated and experimental spectra are compared in Figure 7. The main phosphate group bands (P═O, P−O, and C−O stretching) are quite similar to DMP. However, the $\nu(C_2-O_2)$ band in IR and Raman spectra is well-separated from $\nu(C_1-O_1)$. As for DMP, the MD/DFT simulations (trace B) explain well the main experimental features, whereas the DFT/CPCM simulation (trace A) is less realistic. Spectra of individual EMP conformers (Figure S7) do not show significant variations, similarly as for DMP (Figure S6). The 19 cm^{-1} shift of the $\nu(P{=}O)_{as}$ IR band 2 observed above for DMP is exhibited by the EMP ggt and gtt conformers as well. The band has a similar position in gtt and ttt, the latter form is populated only weakly.

Finally, the simulated and experimental EMSP spectra are plotted in Figure 8. The MD-based results are the most realistic again. However, the plain DFT/CPCM computations in this case describe the experiment reasonably well, too. This may be partially caused by the absence of symmetric and asymmetric vibrations in EMSP, spectral shapes of which the DFT/CPCM method could not reproduce for DMP and EMP. Many EMSP bands simulated by the MD/DFT procedure are somewhat broader than in the experiment, as we have already observed for DMP and EMP, indicating thus insufficient accuracy of the MD force field in this respect.

The $\nu(P{=}S)$ vibration 6 calculated at 634 cm^{-1} is not accessible by IR with BaF_2 cell windows but is observed in the experimental Raman spectra at 647 cm^{-1} (Figure 8). Note that its intensity is lower in IR and much higher in Raman than for $\nu(P{=}O)$ and can be used as an important marker band of the thio-substitution in the phosphate group. The most intense IR bands arise from $\nu(P{=}O)$, $\nu(P-O)$, and $\nu(C-O)$ vibrations (bands 2−5, see Table 1 for a detailed assignment).

Surprisingly, IR spectra of nine main EMSP conformers (Figure S8) vary more than for individual DMP and EMP conformations. For example, position of the $\nu(P{=}O)$ (2) and $\nu(P-O_2)$ (4) bands varies within 20 cm^{-1}. Band 3 has two components, $\nu(C_1-O_1)$ and $\nu(C_2-O_2)$, intensity of which is conformer-dependent as well, so is the $\nu(P-O_1)$ vibration (5) coupled with other modes and split into two components. As an extreme example, the position of the $\nu(P{=}S)$ band (6) is the most sensitive to the geometry and shifts by up to 50 cm^{-1}. This again makes it an excellent marker also for conformer studies of thio-substituted DNA and related systems. For example, the splitting of band 6 in the experimental Raman spectrum (Figure 8) clearly indicates a multiconformer equilibrium, which is confirmed by the broad multicomponent $\nu(C-O)$ (3) and $\nu(P-O_1)$ (5) bands in the IR spectrum.

■ CONCLUSIONS

On several experimental and theoretical models, we investigated vibrational properties of the phosphate and thiphosphate moieties in order to understand their spectral response. The results can also find immediate applications in structural studies of nuclei acids. IR and Raman spectra of the dimethylphosphate, ethylmethylphosphate, ethylmethylthiophosphate molecules were measured and calculated using several methodologies. The combination of molecular dynamics and density functional theory appeared as the best approach, well capturing the effects of environment and dynamics. In particular, the averaging of MD clusters provided spectra significantly improved in comparison with those generated with the dielectric solvent models only.

The GAFF force field produced notably more realistic results than Amber99, which was explained by the Amber99 bias toward canonical DNA geometry. A detailed analysis provided insight into the conformational flexibility of the model molecules and allowed us to identify marker bands particularly sensitive to the conformation. Both the water and phosphate/thiophosphate dynamics were found important for the spectral shapes. The IR spectra appeared to be more sensitive to the environment and conformational dynamics than Raman spectra, which was ascribed to the relatively large dipole moment change characteristic for the P═O/C−O stretching vibrations. The results also cast light on the sensitivity of the phosphate spectral signal to DNA conformation observed previously and explain the shift of P═O asymmetric stretching IR band used for a long time as a marker for B-Z DNA transition. Similar high conformational sensitivity of the P═S stretching band in EMSP indicates that this vibration can serve as a local structural marker for thio-substituted NAs. We thus hope that the more detailed insight into the phosphate vibrations will enhance future spectroscopic and structural DNA studies.

■ ASSOCIATED CONTENT

Ⓢ Supporting Information

The Supporting Information is available free of charge on the ACS Publications website at DOI: 10.1021/acs.jpcb.5b05124.

Synthesis and characterization of EMP and EMSP, calculated geometries, and other computational details. (PDF).

■ AUTHOR INFORMATION

Corresponding Authors

*E-mail: vandrush@uochb.cas.cz.

*E-mail: bour@uochb.cas.cz.

Present Address

(L.B.) Department of Chemistry, Technische Universität Berlin, Straße des 17. Juni 135, 10623 Berlin, Germany.

Notes

The authors declare no competing financial interest.

■ ACKNOWLEDGMENTS

The work was supported by the Grant Agency (13-26526S, P208/11/0105, 13-03978S and 15-09072S) and Academy of Sciences (M200550902) of the Czech Republic. Computational resources were partially provided by the MetaCentrum under the program LM2010005 and the CERIT-SC under the program Centre CERIT Scientific Cloud, part of the Operational Program Research and Development for Innovations, Reg. no. CZ.1.05/3.2.00/08.0144.

■ REFERENCES

(1) Tsuboi, M. Application of Infrared Spectroscopy to Structure Studies of Nucleic Acids. *Appl. Spectrosc. Rev.* **1970**, *3*, 45−90.

(2) Hartman, K. A.; Lord, R. C.; Thomas, G. J. Structural Studies of Nucleic Acids and Polynucleotides by Infrared and Raman Spectroscopy. In *Physico-Chemical Properties of Nucleic Acids*; Duchesne, J., Ed.; Academic Press: New York, 1973; pp 1−89.

(3) Taillandier, E.; Liquier, J.; Taboury, J. A. Infrared Spectral Studies of DNA Conformations. In *Advances in Infrared and Raman Spectroscopy*; Clark, R. J. H., Hester, R. E., Eds.; Wiley-Heyden: New York, 1985; Vol. *12*; pp 65−114.

(4) Blagoi, Y.; Gladchenko, G.; Nafie, L. A.; Freedman, T. B.; Sorokin, V.; Valeev, V.; He, Y. Phase Equilibrium in Poly(rA)·Poly(rU) Complexes with Cd^{2+} and Mg^{2+} Ions Studied by Ultraviolet, Infrared, and Vibrational Circular Dichroism Spectroscopy. *Biopolymers* **2005**, *78*, 275−286.

(5) Gulotta, M.; Goss, D. J.; Diem, M. IR Vibrational CD in Model Deoxyoligonucleotides: Observation of the B→Z Phase Transition and Extended Coupled Oscillator Intensity Calculations. *Biopolymers* **1989**, *28*, 2047−2058.

(6) Keiderling, T. A. Vibrational Circular Dichroism. Applications to Conformational Analysis of Biomolecules. In *Circular Dichroism and the Conformational Analysis of Biomolecules*; Fasman, G. D., Ed.; Plenum Press: New York, 1996; pp 555−597.

(7) Nafie, L. A. Infrared and Raman Vibrational Optical Activity: Theoretical and Experimental Aspects. *Annu. Rev. Phys. Chem.* **1997**, *48*, 357−386.

(8) Barron, L. D.; Zhu, F.; Hecht, L. Raman Optical Activity: An Incisive Probe of Chirality, and of Biomolecular Structure and Behaviour. *Vib. Spectrosc.* **2006**, *42*, 15−24.

(9) Zhong, W. X.; Gulotta, M.; Goss, D. J.; Diem, M. DNA Solution Conformation via Infrared Circular Dichroism: Experimental and Theoretical Results for B-Family Polymers. *Biochemistry* **1990**, *29*, 7485−7491.

(10) Wang, L.; Keiderling, T. A. Vibrational Circular Dichroism Studies of the A-to-B Conformational Transition in DNA. *Biochemistry* **1992**, *31*, 10265−10271.

(11) Xiang, T.; Goss, D. J.; Diem, M. Strategies for the Computation of Infrared CD and Absorption Spectra of Biological Molecules: Ribonucleic Acids. *Biophys. J.* **1993**, *65*, 1255−1261.

(12) Andrushchenko, V.; Wieser, H.; Bouř, P. B-Z Conformational Transition of DNA Monitored by Vibrational Circular Dichroism. Ab Initio Interpretation of the Experiment. *J. Phys. Chem. B* **2002**, *106*, 12623−12634.

(13) Andrushchenko, V.; Wieser, H.; Bouř, P. RNA Structural Forms Studied by Vibrational Circular Dichroism: Ab Initio Interpretation of the Spectra. *J. Phys. Chem. B* **2004**, *108*, 3899−3911.

(14) Andrushchenko, V.; Bouř, P. Applications of the Cartesian Coordinate Tensor Transfer Technique in the Simulations of Vibrational Circular Dichroism Spectra of Oligonucleotides. *Chirality* **2010**, *22*, E96−E114.

(15) Andrushchenko, V.; Tsankov, D.; Krasteva, M.; Wieser, H.; Bouř, P. Spectroscopic Detection of DNA Quadruplexes by Vibrational Circular Dichroism. *J. Am. Chem. Soc.* **2011**, *133*, 15055−15064.

(16) Banyay, M.; Sarkar, M.; Graslund, A. A Library of IR Bands of Nucleic Acids in Solution. *Biophys. Chem.* **2003**, *104*, 477−488.

(17) Benda, L.; Schneider, B.; Sychrovský, V. Calculating the Response of NMR Shielding Tensor $\Sigma(^{31}P)$ and $^2J(^{31}P, ^{13}C)$ Coupling Constants in Nucleic Acid Phosphate to Coordination of the Mg^{2+} Cation. *J. Phys. Chem. A* **2011**, *115*, 2385−2395.

(18) Přecechtělová, J.; Novák, P.; Munzarová, M. L.; Kaupp, M.; Sklenář, V. Phosphorus Chemical Shifts in a Nucleic Acid Backbone from Combined Molecular Dynamics and Density Functional Calculations. *J. Am. Chem. Soc.* **2010**, *132*, 17139−17148.

(19) Florián, J.; Baumruk, V.; Štrajbl, M.; Bednárová, L.; Štěpánek, J. IR and Raman Spectra, Conformational Flexibility, and Scaled Quantum Mechanical Force Fields of Sodium Dimethyl Phosphate and Dimethyl Phosphate Anion. *J. Phys. Chem.* **1996**, *100*, 1559−1568.

(20) Florián, J.; Štrajbl, M.; Warshel, A. Conformational Flexibility of Phosphate, Phosphonate, and Phosphorothioate Methyl Esters in Aqueous Solution. *J. Am. Chem. Soc.* **1998**, *120*, 7959−7966.

(21) Eckert, F.; Klamt, A. Fast Solvent Screening via Quantum Chemistry: COSMO-RS Approach. *AIChE J.* **2002**, *48*, 369−385.

(22) Klamt, A. COSMO and COSMO-RS. In *The Encyclopedia of Computational Chemistry*; Schleyer, P. R., Allinger, N. L., Clark, T.,

Gasteiger, J., Kollman, P. A., Schaefer, H. F., III, Schreiner, P. R., Eds.; John Wiley & Sons: Chichester, 1998; Vol. *1*; pp 604−615.

(23) Bouř, P.; Michalík, D.; Kapitán, J. Empirical Solvent Correction for Multiple Amide Group Vibrational Modes. *J. Chem. Phys.* **2005**, *122*, 144501.

(24) Bouř, P.; Andrushchenko, V.; Kabeláč, M.; Maharaj, V.; Wieser, H. Simulations of Structure and Vibrational Spectra of Deoxyoctanucleotides. *J. Phys. Chem. B* **2005**, *109*, 20579−20587.

(25) Andrushchenko, V.; Bouř, P. Infrared Absorption Detection of Metal Ion-Deoxyguanosine Monophosphate Binding: Experimental and Theoretical Study. *J. Phys. Chem. B* **2009**, *113*, 283−291.

(26) Přecechtělová, J.; Munzarová, M. L.; Vaara, J.; Novotný, J.; Dračínský, M.; Sklenář, V. Toward Reproducing Sequence Trends in Phosphorus Chemical Shifts for Nucleic Acids by MD/DFT Calculations. *J. Chem. Theory Comput.* **2013**, *9*, 1641−1656.

(27) Šípová, H.; Springer, T.; Rejman, D.; Šimák, O.; Petrová, M.; Novák, P.; Rosenbergová, S.; Páv, O.; Liboska, R.; Barvík, I.; et al. 5 ′-O-Methylphosphonate Nucleic Acids-New Modified DNAs That Increase the Escherichia Coli RNAse H Cleavage Rate of Hybrid Duplexes. *Nucleic Acids Res.* **2014**, *42*, 5378−5389.

(28) Watts, J. K.; Corey, D. R. Silencing Disease Genes in the Laboratory and the Clinic. *J. Pathol.* **2012**, *226*, 365−379.

(29) Caricato, M.; Ingrosso, F.; Mennucci, B.; Tomasi, J. A Time-Dependent Polarizable Continuum Model: Theory and Application. *J. Chem. Phys.* **2005**, *122*, 154501.

(30) Mennucci, B. Modeling Environment Effects on Spectroscopies through QM/Classical Models. *Phys. Chem. Chem. Phys.* **2013**, *15*, 6583−6594.

(31) Hopmann, K. H.; Ruud, K.; Pecul, M.; Kudelski, A.; Dračínský, M.; Bouř, P. Explicit Versus Implicit Solvent Modeling of Raman Optical Activity Spectra. *J. Phys. Chem. B* **2011**, *115*, 4128−4137.

(32) Ramírez, R.; López-Ciudad, T.; Kumar, P.; Marx, D. Quantum Corrections to Classical Time-Correlation Functions: Hydrogen Bonding and Anharmonic Floppy Modes. *J. Chem. Phys.* **2004**, *121*, 3973−3983.

(33) Everitt, K. F.; Geva, E.; Skinner, J. L. Determining the Solvation Correlation Function from Three-Pulse Photon Echoes in Liquids. *J. Chem. Phys.* **2001**, *114*, 1326−1335.

(34) Jiang, L.; Sun, S.; Heine, N.; Liu, J.; Yacovitch, T. I.; Wende, T.; Liu, Z.; Neumark, D. M.; Asmis, K. R. Large Amplitude Motion in Cold Monohydrated Dihydrogen Phosphate Anions $H_2PO_4^-(H_2O)$: Infrared Photodissociation Spectroscopy Combined with Ab Initio Molecular Dynamics Simulations. *Phys. Chem. Chem. Phys.* **2014**, *16*, 1314−1318.

(35) Cimas, A.; Maitre, P.; Ohanessian, G.; Gaigeot, M. P. Molecular Dynamics and Room Temperature Vibrational Properties of Deprotonated Phosphorylated Serine. *J. Chem. Theory Comput.* **2009**, *5*, 2388−2400.

(36) Case, D. A.; Darden, T. A.; Cheatham III, T. E.; Simmerling, C. L.; Wang, J.; Duke, R. E.; Luo, R.; Walker, R. C.; Zhang, W.; Merz, K. M. et al. *Amber Tools 12*; University of California: San Francisco, 2012.

(37) Bayly, C. I.; Cieplak, P.; Cornell, W. D.; Kollman, P. A. A Well-Behaved Electrostatic Potential Based Method Using Charge Restraints for Deriving Atomic Charges - the RESP Model. *J. Phys. Chem.* **1993**, *97*, 10269−10280.

(38) Dupradeau, F. Y.; Pigache, A.; Zaffran, T.; Savineau, C.; Lelong, R.; Grivel, N.; Lelong, D.; Rosanski, W.; Cieplak, P. The R.Ed. Tools: Advances in RESP and ESP Charge Derivation and Force Field Library Building. *Phys. Chem. Chem. Phys.* **2010**, *12*, 7821−7839.

(39) Vanquelef, E.; Simon, S.; Marquant, G.; Garcia, E.; Klimerak, G.; Delepine, J. C.; Cieplak, P.; Dupradeau, F. Y. Red Server: A Web Service for Deriving RESP and ESP Charges and Building Force Field Libraries for New Molecules and Molecular Fragments. *Nucleic Acids Res.* **2011**, *39*, W511−W517.

(40) Case, D. A.; Darden, T. A.; Cheatham III, T. E.; Simmerling, C. L.; Wang, J.; Duke, R. E.; Luo, R.; Crowley, M.; Walker, R. C.; Zhang, W. et al. *Amber 10*; University of California: San Francisco, 2008.

(41) Perez, A.; Marchan, I.; Svozil, D.; Šponer, J.; Cheatham, T. E.; Laughton, C. A.; Orozco, M. Refinenement of the Amber Force Field for Nucleic Acids: Improving the Description of α/Γ Conformers. *Biophys. J.* **2007**, *92*, 3817−3829.

(42) Jorgensen, W. L.; Chandrasekhar, J.; Madura, J. D.; Impey, R. W.; Klein, M. L. Comparison of Simple Potential Functions for Simulating Liquid Water. *J. Chem. Phys.* **1983**, *79*, 926−935.

(43) Grossfield, A. *Wham: An Implementation of the Weighted Histogram Analysis Method*, version 2.0.9; Rochester University: Rochester, NY, 2013.

(44) IBM Corp. *CPMD V3.11*; MPI für Festkörperforschung: Stuttgart, 1997−2001.

(45) Becke, A. D. Density-Functional Thermochemistry. III. The Role of Exact Exchange. *J. Chem. Phys.* **1993**, *98*, 5648−5652.

(46) Frisch, M. J.; Trucks, G. W.; Schlegel, H. B.; Scuseria, G. E.; Robb, M. A.; Cheeseman, J. R.; Scalmani, G.; Barone, V.; Mennucci, B.; Petersson, G. A. et al. *Gaussian 09*, revision A.02; Gaussian, Inc.: Wallingford, CT, 2009.

(47) Ahlrichs, R.; Bar, M.; Haser, M.; Horn, H.; Kolmel, C. Electronic-Structure Calculations on Workstation Computers - the Program System Turbomole. *Chem. Phys. Lett.* **1989**, *162*, 165−169.

(48) Becke, A. D. A New Mixing of Hartree−Fock and Local Density-Functional Theories. *J. Chem. Phys.* **1993**, *98*, 1372−1377.

(49) Klamt, A.; Schuurmann, G. COSMO - a New Approach to Dielectric Screening in Solvents with Explicit Expressions for the Screening Energy and Its Gradient. *J. Chem. Soc., Perkin Trans. 2* **1993**, *5*, 799−805.

(50) Barone, V.; Cossi, M.; Tomasi, J. Geometry Optimization of Molecular Structures in Solution by the Polarizable Continuum Model. *J. Comput. Chem.* **1998**, *19*, 404−417.

(51) Scalmani, G.; Frisch, M. J. Continuous Surface Charge Polarizable Continuum Models of Solvation. I. General Formalism. *J. Chem. Phys.* **2010**, *132*, 114110.

(52) Klamt, A. Conductor-Like Screening Models for Real Solvents: A New Approach to the Quantitative Calculation of Solvation Phenomena. *J. Phys. Chem.* **1995**, *99*, 2224−2235.

(53) Grimme, S.; Antony, J.; Ehrlich, S.; Krieg, H. A Consistent and Accurate Ab Initio Parametrization of Density Functional Dispersion Correction (DFT-D) for the 94 Elements H-Pu. *J. Chem. Phys.* **2010**, *132*, 154104.

(54) Becke, A. D.; Johnson, E. R. Exchange-Hole Dipole Moment and the Dispersion Interaction. *J. Chem. Phys.* **2005**, *123*, 154101.

(55) Grimme, S. Supramolecular Binding Thermodynamics by Dispersion-Corrected Density Functional Theory. *Chem. - Eur. J.* **2012**, *18*, 9955−9964.

(56) Katsyuba, S.; Vandyukova, E. Scaled Quantum Mechanical Computations of Vibrational Spectra of Organoelement Molecules, Containing the Atoms P, S, and Cl. *Chem. Phys. Lett.* **2003**, *377*, 658−662.

(57) Hudecová, J.; Hopmann, K. H.; Bouř, P. Correction of Vibrational Broadening in Molecular Dynamics Clusters with the Normal Mode Optimization Method. *J. Phys. Chem. B* **2012**, *116*, 336−342.

(58) Li, X. J.; Hopmann, K. H.; Hudecová, J.; Stensen, W.; Novotná, J.; Urbanová, M.; Svendsen, J. S.; Bouř, P.; Ruud, K. Absolute Configuration of a Cyclic Dipeptide Reflected in Vibrational Optical Activity: Ab Initio and Experimental Investigation. *J. Phys. Chem. A* **2012**, *116*, 2554−2563.

(59) Hopmann, K. H.; Šebestik, J.; Novotná, J.; Stensen, W.; Urbanová, M.; Svenson, J.; Svendsen, J. S.; Bouř, P.; Ruud, K. Determining the Absolute Configuration of Two Marine Compounds Using Vibrational Chiroptical Spectroscopy. *J. Org. Chem.* **2012**, *77*, 858−869.

(60) Bouř, P.; Keiderling, T. A. Partial Optimization of Molecular Geometry in Normal Coordinates and Use as a Tool for Simulation of Vibrational Spectra. *J. Chem. Phys.* **2002**, *117*, 4126−4132.

(61) Saenger, W. *Principles of Nucleic Acid Structure*; Springer-Verlag: New York, 1984.

(62) Schneider, B.; Neidle, S.; Berman, H. M. Conformations of the Sugar-Phosphate Backbone in Helical DNA Crystal Structures. *Biopolymers* **1997**, *42*, 113−124.

(63) Schneider, B.; Morávek, Z.; Berman, H. M. RNA Conformational Classes. *Nucleic Acids Res.* **2004**, *32*, 1666−1677.

(64) MacKerell, A. D. Influence of Water and Sodium on the Energetics of Dimethylphosphate and Its Implications for DNA Structure. *J. Chim. Phys. Phys. Chim. Biol.* **1997**, *94*, 1436−1447.

(65) Schwalbe, C. H.; Goody, R.; Saenger, W. Crystal and Molecular-Structure of Tetraphyridine-Bis(Diethylphohorothioato) Magnesium-(II), a Model Substance for Polynucleotide Phosphorothioates. *Acta Crystallogr., Sect. B: Struct. Crystallogr. Cryst. Chem.* **1973**, *29*, 2264−2272.

(66) Andrushchenko, V.; Leonenko, Z.; Cramb, D.; van de Sande, H.; Wieser, H. Vibrational CD (VCD) and Atomic Force Microscopy (AFM) Study of DNA Interaction with Cr^{3+} Ions: VCD and AFM Evidence of DNA Condensation. *Biopolymers* **2002**, *61*, 243−260.

(67) Taillandier, E.; Liquier, J. Infrared Spectroscopy of DNA. *Methods Enzymol.* **1992**, *211*, 307−335.

(68) Loprete, D. M.; Hartman, K. A. Conditions for the Stability of the B, C, and Z Structural Forms of Poly(dG-dC) in the Presence of Lithium, Potassium, Magnesium, Calcium, and Zinc Cations. *Biochemistry* **1993**, *32*, 4077−4082.

(69) Tajmir-Riahi, H. A.; Neault, J. F.; Naoui, M. Does DNA Acid Fixation Produce Left-Handed Z Structure? *FEBS Lett.* **1995**, *370*, 105−108.

(70) Gessner, R. V.; Frederick, C. A.; Quigley, G. J.; Rich, A.; Wang, A. H. J. The Molecular-Structure of the Left-Handed Z-DNA Double Helix at 1.0 Å Atomic Resolution - Geometry, Conformation, and Ionic Interactions of d(CGCGCG). *J. Biol. Chem.* **1989**, *264*, 7921−7935.

(71) Schwabe, T.; Grimme, S. Towards Chemical Accuracy for the Thermodynamics of Large Molecules: New Hybrid Density Functionals Including Non-Local Correlation Effects. *Phys. Chem. Chem. Phys.* **2006**, *8*, 4398−4401.

(72) Daněček, P.; Kapitán, J.; Baumruk, V.; Bednárová, L.; Kopecký, V., Jr.; Bouř, P. Anharmonic Effects in IR, Raman and Raman Optical Activity Spectra of Alanine and Proline Zwitterions. *J. Chem. Phys.* **2007**, *126*, 224513.

(73) Samsonyuk, A.; Scheurer, C. Configuration Space Partitioning and Matrix Buildup Scaling for the Vibrational Configuration Interaction Method. *J. Comput. Chem.* **2013**, *34*, 27−37.

(74) Bouř, P.; Michalík, D.; Kapitán, J. Empirical Solvent Correction for Multiple Amide Group Vibrational Modes. *J. Chem. Phys.* **2005**, *122*, 144501.